IIETA International Information and Engineering Technology Association
Advancing the World of Information and Engineering

Traitement du Signal
Vol. 36, No. 2, April, 2019, pp. 127-132
Journal homepage: http://iieta.org/journals/ts

Diagnosis of an Inverter IGBT Open-circuit Fault by Hilbert-Huang Transform Application

Bilal Djamal Eddine Cherif[1*], Azeddine Bendiabdellah[1], Mostefa Tabbakh[2]

[1] Diagnosis Group, Laboratory LDEE, Electrical Engineering Faculty, University of Sciences and Technology of Oran, Oran 31000, Algeria
[2] Department of Electrical Engineering, University of M'sila, M'sila 28000, Algeria

Corresponding Author Email: cherif.doc84@gmail.com

https://doi.org/10.18280/ts.360201

Received: 12 January 2019
Accepted: 29 March 2019

Keywords:
inverter, IGBT, open-circuit, HHT, EMD, CEEMDAN, IMF, spectral envelope, RMS

ABSTRACT

The open-circuit fault of an inverter IGBT switch leads to total or partial loss of control of the phase currents resulting in the dysfunction of the system. Moreover, if the fault is not detected and compensated quickly, it can cause complete shutdown of the system. To ensure the system service continuity, efficient and fast techniques for detecting and locating the open-circuit fault of the IGBT must be implemented. This paper proposes a Hilbert-Huang Transform (HHT) based on the detection of the IGBT open-circuit fault. The proposed technique is based on the complete empirical mode decomposition with adaptive noise (CEEMDAN). This mode is applied to the motor stator current signals to obtain a function called the intrinsic mode function (IMF). The IMF contains the frequency (and its multiples) related to the frequency of the harmonic characterizing the IGBT switch open-circuit fault of the inverter. In order to test the effectiveness of the proposed technique and validate the results, several experimental tests are performed using a test bench.

1. INTRODUCTION

In general, maintenance is intended to ensure the maximum availability of production equipment at an optimal cost under good conditions of quality and safety. The general principle of the diagnostic algorithms is based on the use of the data recorded on the system and the knowledge that one possesses of its healthy operation (for the detection) or its faulty operation (for the location). These algorithms develop symptoms that reveal the faulty behavior and the nature of the dysfunction. In this framework, static converters, particularly inverters, are mainly present in variable speed electrical drive systems. Reliability data; from the literature; justify the envisaged scope for the implementation of fault tolerance or failure. Figure 1 shows the distribution of faults in% in an inverter [1].

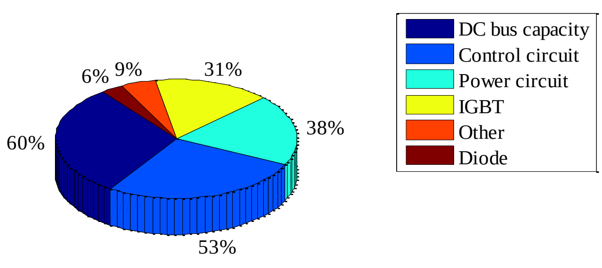

Figure 1. Distribution of faults in % in a static converter

Among these diagnostic methods there are spectral analysis techniques based on the Fourier transform (FT). The FT provides a good description of the stationary and pseudo-stationary signals but has many limitations when the signals to be analyzed are not stationary. In this case, the solution would be to use the so-called time-frequency analysis tools. These methods include: the STFT and the Hilbert-Huang Transform (HHT) [2].

The authors Hilbert and Huang have recently proposed a technique that approaches in another angle the problematic of non-stationary signal analysis with the empirical modal decomposition (EMD) approach. The EMD adaptively decomposes a signal in a sum of oscillating components. Unlike FT or wavelets, the basis of the EMD decomposition is intrinsic to the signal. One of the motivations for the development of the EMD is the estimation of the instantaneous frequency (IF) of the signal. Indeed, the conventional approach of estimating the IF based on the Hilbert transformation (HT) is strictly limited to single-component signals. Thus, constraints are imposed on these oscillating components to correctly estimate the IF (with a physical sense) specific to each component present in the signal. The EMD combined with the HT or another method of estimating the IF results in a time-frequency representation (TFR). The EMD is defined by a process called sifting, which decomposes the signal into basic contributions called empirical modes or intrinsic mode functions (IMF). These are signals of amplitude modulation - frequency modulation type mono-component (in broad sense) each of zero average. The principle of the EMD is based on an adapted decomposition describing the signal locally as a succession of contributions of fast oscillations (high frequencies) on slower oscillations (low frequencies) [3-6].

Several papers have been published in this diagnostic field based on the HHT. The author in the paper [7] presents a method using the spectral envelope of the stator current for the online automatic detection of broken bar faults. In this paper, the HHT is used to estimate the severity of faults for different loads using classification techniques. The spectral envelope of the stator current makes it possible to read the frequency relative to the fault, which confirms the existence of the fault. The author [8] proposes a method based on the complete empirical ensemble mode decomposition with adaptive noise (CEEMDAN) associated with an optimized Thresholding operation. The CEEMDAN is first applied to the vibration signals to obtain a series of functions called the IMF functions. An approach based on the energy content of each mode with the white noise characteristic is then proposed to determine the trigger point to select the relevant modes. The author in paper [9] presents a rolling fault diagnosis method based on an improvement time-time of Hilbert (HTT a derivative of the HHT) with the main component which is the Denoising HTT transform matrix. The HTT was performed on vibration signals to deduce the transformed matrix. The main component is then used to attenuate the noise of the HHT matrix in order to improve its robustness and extract information and characteristics of the bearing fault.

This paper proposes an HHT-based diagnostic method for detecting the open-circuit fault of an IGBT in an inverter. The proposed technique is based on complete ensemble empirical mode decomposition with an Adaptive Noise (CEEMDAN). This mode is applied to the motor stator current signals to obtain a function called the intrinsic mode function (IMF) containing the frequency of the harmonic relative to the harmonic characterizing the IGBT fault. In order to test the effectiveness of the proposed technique and validate the results, several experimental tests are carried out on the system using a practical test bench at our LDEE laboratory, consisting of an induction motor powered by a two-level three-phase faulty voltage inverter controlled by the MLI-SVM strategy.

2. HILBERT-HUANG TRANSFORM

In this section, the principle of HHT will be presented as well as the different versions of decomposition in empirical modes (EMD and CEEMDAN) in addition to the spectral envelope and RMS.

2.1 EMD algorithm

The EMD method decomposes the signal into a finite number of IMFs and a residue. It should satisfy the following conditions [10]:

1) The number of extrema and the number of zero-crossings are equal or differ by one.

2) The mean value of the envelopes defined by local maxima and local minima is zero.

For a given signal(t) , the EMD algorithm is described in the following steps [10]:

1st step: Initialize: $r_0 = (x(t))$ and $i=1$

2nd step: Extract the *iIMF*.

(a) Initialize $h_{i(k-1)} = r_i$, $k=1$.

(b) Extract the local Max and Min of $h_{i(k-1)}$.

(c) Interpolate the local Max and Min with cubic spleen lines to form the upper and lower envelopes of $h_{i(k-1)}$.

(d) Calculate the average $m_{i(k-1)}$ of the upper and lower envelopes of $h_{i(k-1)}$.

(e) Let $h_{ik} = h_{i(k-1)} - m_{i(k-1)}$.

(f) If h_{ik} is an IMF, set $IMF_i=h_{ik}$, otherwise go to step (b) with $k=k+1$.

3rd step: Define $r_{i+1}=r_i-IMF_i$.

4th step: Continue the process until the final residue r_n satisfies the predefined stopping criterion. The stopping condition (*SD*) is calculated from the two consecutive sifting results, namely h_{k-1} and h_k as [9]:

$$SD(i) = \sum_{t=0}^{T} \frac{\left| h_{j,i-1}(t) - h_{j,i}(t) \right|^2}{\left(h_{j,i-1}(t) \right)^2} \tag{1}$$

where: T is the time duration. The sifting process is terminated when the *SD* value is greater than a certain threshold. Here a typical value of *SD* can be set between 0.2 and 0.3 [9].

The signal can be expressed as follows:

$$x(t) = \sum_{i=1}^{n} c_i + r_n \tag{2}$$

2.2 CEEMDAN algorithm

The Complete Empirical Ensemble Mode Decomposition an Adaptive Noise (CEEMDAN) is used to solve the EEMD problem related to residual noise and also to the existence of modes with different numbers. The CEEMDAN algorithm is illustrated by the following steps [11]:

1st step: Use the EMD to decompose I realizations of $x + \varepsilon_0 \omega^i (i = 1, \ldots \ldots, I)$in order to obtain its first modes and to calculate the first mode of the CEEMDAN as follows:

$$\overline{IMF_1} = \frac{1}{I} \sum_{i=1}^{I} E_1\left(x + \zeta \omega_i\right) \tag{3}$$

With x, ω_i: Gaussian white noise with N(0,1), ε: a noise standard deviation, I: Number of sets.

2nd step: Calculate the first residue$r_1 = x - \overline{IMF_1}$.

3rd step: Use the EMD to decompose $r_1 + \varepsilon_1 E_1(\omega^i), (i = 1, \ldots \ldots, I)$ to get its first modes and define the second mode of CEEMDAN as:

$$\overline{IMF_2} = \frac{1}{I} \sum_{i=1}^{I} E_1\left(r_1 + \zeta_1 E_1(\omega^i)\right) \tag{4}$$

4th step: For $k = 2\ldots, k$ the residue is given as follows:

$$r_k = r_{k-1} - \overline{IMF_k} \tag{5}$$

5th step: Use EMD to decompose the realizations $r_k + \varepsilon_k E_k(\omega^i), (i = 1, \ldots \ldots, I)$ and define the $(k + 1)^{th}$CEEMDAN mode as follows:

$$\overline{IMF_{k+1}} = \frac{1}{I} \sum_{i=1}^{I} E_1\left(r_k + \zeta_k E_k(\omega^i)\right) \tag{6}$$

With $E_k(.)$: k^{th}IMF product to obtain par the EMD.

6th step: Go to step 4 for the next k.

7th step: Iterate steps 4-6 until the resulting residue can no longer be decomposed by the EMD. The final residue is given as follows:

$$r_n = x - \sum_{i=1}^{n} \overline{IMF_i} \quad (7)$$

So that the given signal can be expressed by:

$$x = r_n + \sum_{i=1}^{n} \overline{IMF_i} \quad (8)$$

With: n: The total number of modes, ε_k : The amplitude of the added white noise, ω : White noise with the unit variance.

In this paper, the proposed technique is represented by the flowchart of Figure 2 as follows:

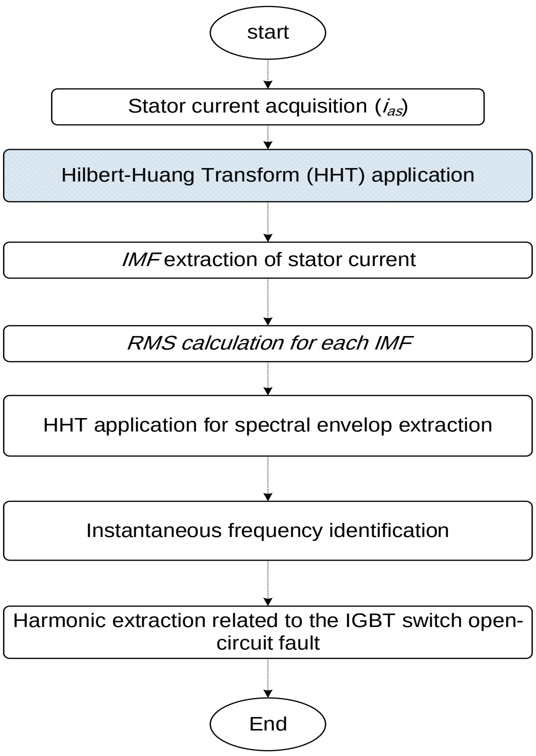

Figure 2. Organizational chart of the proposed method

3. EXPERIMENTAL RESULTS AND INTERPRETATION

The three-phase inverter used is this work is an IGBT-based three-phase (SEMI-KRON) controlled by the DSPACE 1104 Card. The inverter IGBTs are controlled by the MLI-SVM strategy. The motor used is of a three-phase squirrel cage type; with a nominal power of 3 Kw, a frequency of 50 Hz and a nominal rotor speed of 1440 rpm.

This motor is mechanically coupled to a DC generator used as a load. The measuring system has three voltage sensors (TEKTRONIX P5200) and three Hall-Effect current sensors (FLUCK i30s (AC/DC CURRENT CLAMP)), a tachometer (ONO SOKKI HT-341) and an acquisition card (NI-6330). Finally, the whole set is connected to a computer for visualizing the processed acquired signals as shown in the photo of Figure 3 [12].

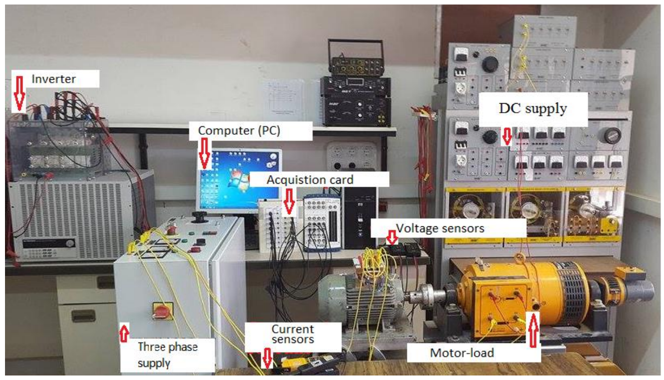

Figure 3. Photo of experimental test-rig [12]

Table 1 presents the induction motor parameters and specifications.

Table 1. Parameters of the induction motor

Rated Power	3 KW
Supply frequency	50 Hz
Rated voltage	380 V
Rated current	7A
Rotor speed	1410 rev/min
Number of rotor bars	28
Number of stator slots	36
Power factor	0.83
Number of pair of poles	2

Figure 4 shows the structure of the two-level three-phase voltage inverter. The system consists of a three-phase voltage inverter with two levels based on faulty IGBT switches supplying an induction machine.

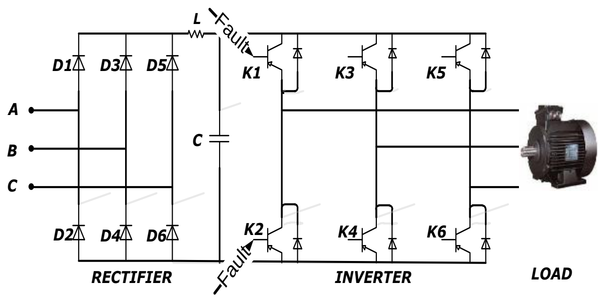

Figure 4. Structure of the converter-motor assembly with open-circuit fault

All the acquisitions were made in nominal mode over a period of 5 seconds with a sampling frequency of 1.5 kHz.

The various modes of operation of an inverter-motor assembly made to validate the diagnostic procedure are:

- Operation with a healthy inverter.
- Operation with an inverter open-circuit fault of IGBT K_1.
- Operation with an inverter open-circuit fault of IGBT K_2.

Figure 5 shows the stator current i_{as} in both the healthy and open-circuit faulty cases.

Figure 5 shows the stator current in the normal and abnormal operation of the system. The stator current is characterized with respect to the normal regime by a sudden variation at the instant of the application of the open-circuit fault at the K_1 switch resulting in a loss of the positive halfcycle of the current. On the other hand, in the case of a fault at the switch K_2, a loss of the negative alternation is observed.

Figure 6 depicts the selected IMFs in the healthy and the open-circuit faulty cases.

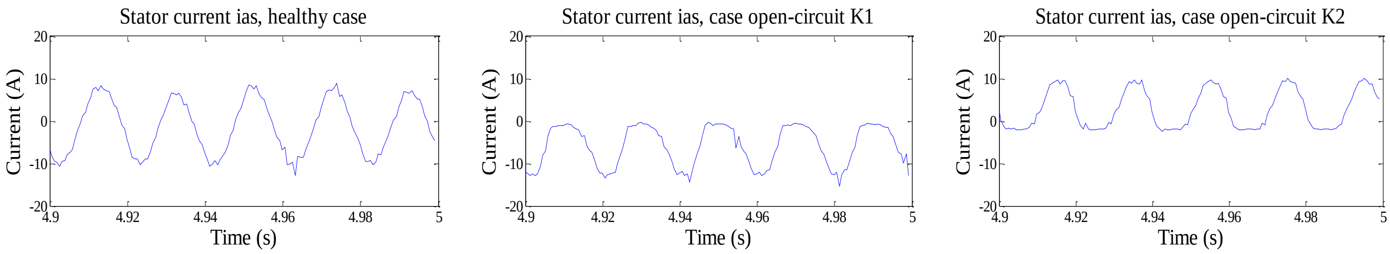

(a) Healthy state (b) Open-circuit at switch K_1 (c) Open-circuit at switch K_2

Figure 5. Stator current

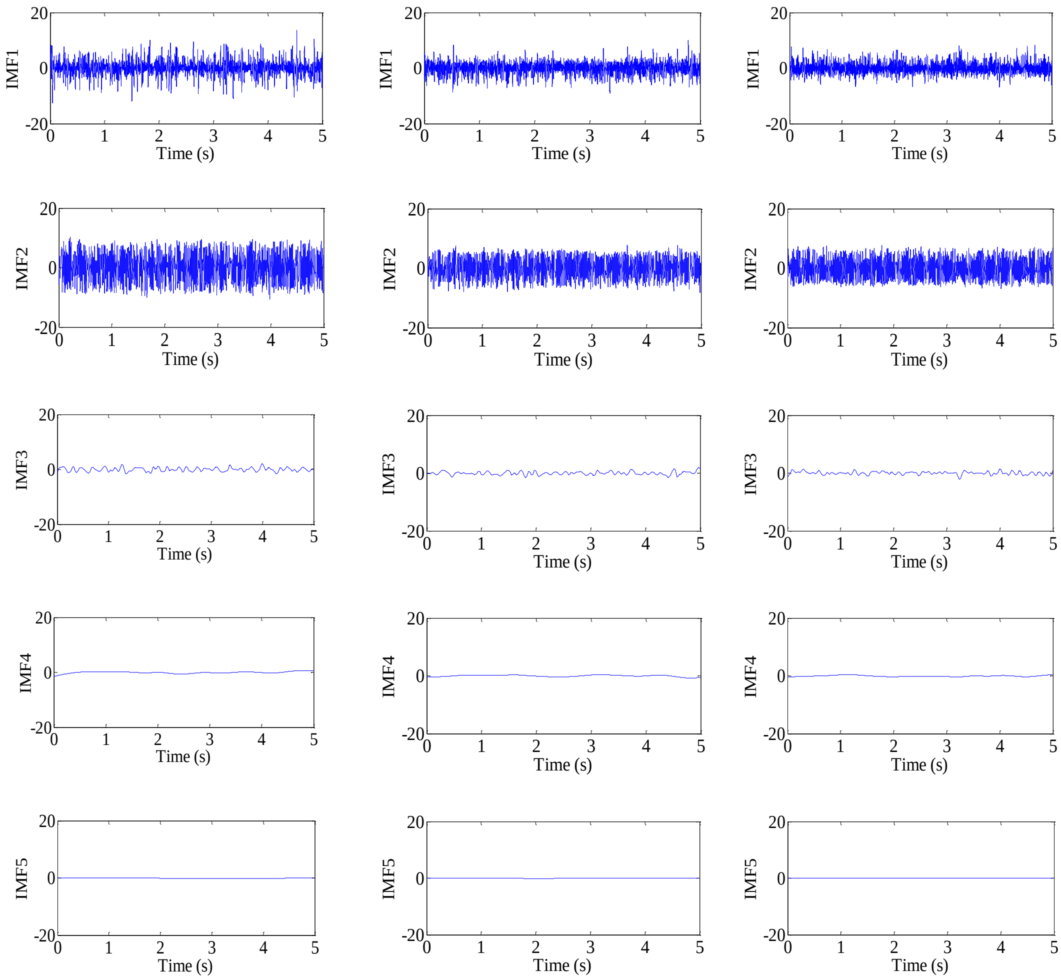

(a) Healthy state (b) Open-circuit at switch K_1 (c) Open-circuit at switch K_2

Figure 6. IMF

3.1 Statistical study

RMS: it is a very characteristic value of the signal, since it has a direct relation with the energy contained in it:

$$RMS = \sqrt{\frac{1}{T}\int_{0}^{t} IMF^{2}(t)dt} \tag{9}$$

where: IMF (t) is the representative function of the signal and "t" is the analysis time.

Table 2 presents the RMS value of each IMF. After analyzing the results obtained in Table 2 for each IMF we observed logic in IMF_1 that identifies the IGBT fault. $K_{1,3,5}$ are always lower than the values $K_{2,4,6}$ respectively in the case of an open-circuit fault. The IMF_1 signal is therefore the one to be used to detect and locate the harmonics that characterizes the open-circuit fault IGBT.

Table 2. RMS value of each IMF

State	IMF_1	IMF_2	IMF_3	IMF_4	IMF_5
Stator current *ias*					
Heathy	82.7486	251.5579	392.6519	93.3259	54.5970
Open K_1	66.5023	188.9364	296.1187	65.0230	44.5439
Open K_2	67.2751	166.4776	292.3342	66.4481	37.1695
Open K_3	95.8056	299.4912	478.9089	104.0427	70.1447
Open K_4	90.9676	290.8385	463.9138	103.9608	55.5179
Open K_5	85.4351	251.0758	439.7275	87.3736	56.3215
Open K_6	85.5871	270.7648	421.8767	96.9308	55.5287
Stator current *ibs*					
Heathy	78.1394	224.4353	400.2280	84.5102	51.3490
Open K_1	83.8776	279.4305	428.2569	98.4593	59.4270
Open K_2	80.4376	259.0379	434.0585	95.5906	63.0193
Open K_3	62.0850	176.8302	293.7399	64.8789	47.8038
Open K_4	64.0776	180.4871	301.9739	66.5300	41.6790
Open K_5	92.9372	276.8886	495.3335	116.2171	68.1189
Open K_6	93.9432	282.5435	474.9952	103.5992	62.0288
Stator current *ics*					
Heathy	80.5750	257.3659	422.6741	99.5111	60.7217
Open K_1	94.2862	289.2505	485.5097	102.1549	59.3271
Open K_2	91.8464	312.2062	478.6916	103.9096	69.4545
Open K_3	82.6258	282.0376	428.4229	102.7446	54.2908
Open K_4	79.8416	262.4210	422.2279	103.5813	56.0183
Open K_5	62.3196	194.9059	297.3967	63.2087	43.7761
Open K_6	65.1510	181.7017	304.8296	68.6557	42.2992

3.2 Hilbert spectral envelope

The characteristics of the Hilbert spectral envelope are quoted as follows:

(a) Elimination of the fundamental (50 Hz) of the current spectrum.

(b) Shifting of all frequency signatures to the left of 50 Hz.

(c) Visibility of the frequency signatures of the faults those are generally of very low amplitude due to the absence of the fundamental.

(d) Visibility of the frequency signatures of faults allowing the use of the linear scale instead of the semi-logarithmic scale.

(e) Elimination of the fundamental; only one characteristic frequency component of the fault appears instead of the three lateral bands multiple of 2. As for example for the signature of the open-circuit fault of an IGBT of the inverter.

Figure 7 shows the IMF spectral envelope in the healthy case and the case of open-circuit fault at the IGBT switches K_1 and K_2.

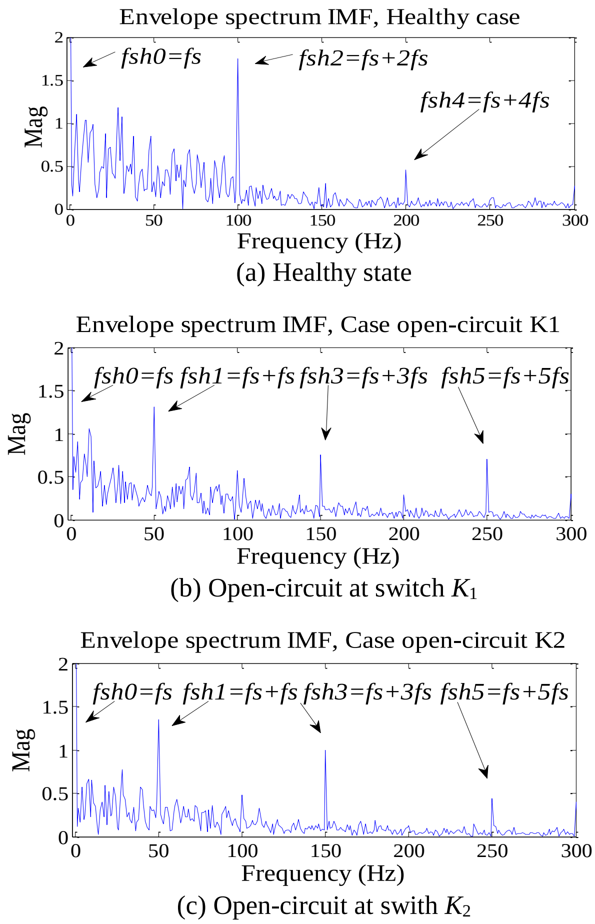

(a) Healthy state

(b) Open-circuit at switch K_1

(c) Open-circuit at swith K_2

Figure 7. Spectral envelope

Figure 7(a), the harmonic f_s is no more visible because of the Hilbert spectral envelope effect that causes the elimination of this harmonic and the shift of all frequencies to the left of the harmonic of 50 Hz. This explains the existence of the harmonics (f_{sh2}) and (f_{sh4}).

In the case of the open-circuit fault of the IGBT switches at K_1 and K_2, depict the existence of the fundamental harmonic f_s (50 Hz) and other harmonics $2f_s$ (100 Hz), $3f_s$ (150 Hz) and $4f_s$ (200 Hz). This explains the existence of the harmonic (f_{sh1}), (f_{sh3}) and (f_{sh5}) in the Hilbert spectral envelope shown in Figure 7(b) and 7(c) hence replacing the harmonic ($f_s + f_s$), ($f_s + 3f_s$) and ($f_s + 5f_s$) with a shifting of 50 Hz.

Table 3 summarizes the amplitudes of the harmonics (f_{sh1}, f_{sh2}, f_{sh3}, f_{sh4} and f_{sh5}) of the spectral envelope in the healthy and the IGBT open-circuit faulty cases.

Table 3. Amplitude of the (f_{sh1}, f_{sh2}, f_{sh3}, f_{sh4} and f_{sh5}) of spectral envelope

Harmonics	f_{sh1}(dB)	f_{sh2} (dB)	f_{sh3} (dB)	f_{sh4} (dB)	f_{sh5} (dB)	f_{inst} (Hz)
Healthy case	0	1.746	0	0.4605	0	0
Open K_1	1.309	0	0.7544	0	0.707	50
Open K_2	1.344	0	0.9951	0	0.4363	50
Open K_3	0.8918	0	0.8079	0	0.4424	50
Open K_4	1.329	0	0.7949	0	0.7329	50
Open K_5	1.268	0	1.04	0	0.5924	50
Open K_6	1.316	0	0.7719	0	0.615	50

According to Table 3, a comparative analysis between the healthy and the IGBT open-circuit fault cases clearly shows a frequency signature at about (50Hz) for the Hilbert spectral envelope. It should be noted that this frequency is the one that characterizes the open-circuit fault of the IGBT. In order to confirm the validity of this observation, the instantaneous Hilbert frequency is identified and shown in Figure 8.

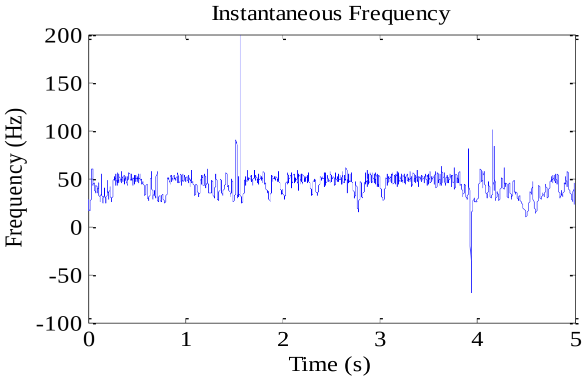

Figure 8. Instantaneous frequency of HHT in case of open-circuit fault of switches at K_1 and K_2

Figure 8 shows that the instantaneous frequency (f_{sh1}=50 Hz) is the frequency that characterizes the open-circuit fault of the IGBT.

4. CONCLUSIONS

In this paper, a method for diagnosing and detecting the harmonic characteristic of the open-circuit fault of an IGBT of the two-stage three-phase inverter supplying an induction motor is proposed. This diagnostic method is based on the Hilbert-Huang transform to identify the instantaneous frequency that allows us to detect the frequency characterizing the open-circuit fault of the IGBT. This paper study is based on the extraction of the IMF for the healthy and the IGBT open-circuit fault cases by using the algorithm (CEEMDAN). To detect the open-circuit faults related to the resulting IMF, the Hilbert spectral envelope are conducted to identify the instantaneous frequency. This instantaneous frequency is the frequency characterizing the open-circuit fault of the IGBT. The method proposed is more efficient and more sensitive to the early detection and the diagnosis of open-circuit fault of the IGBTs of the inverter when compared to the conventional methods for example the wavelet or the STFT. The various results obtained are validated by several experimental works carried out in the LDEE laboratory by the diagnostic group to assess the effectiveness and the merits of the proposed HHT approach.

REFERENCES

[1] Kakurin, A.M., Orlovsky, I.I. (2005). Hilbert-Huang transform in MHD plasma diagnostics. Plasma Physics Reports, 31(12): 1054-1063. https://doi.org/10.1134/1.2147651

[2] Neto, E.P.S., Custaud, M.A., Cejka, J.C., Abry, P., Frutoso, J., Gharib, C., Flandrin, P. (2004). Assessment of cardiovascular autonomic control by the empirical mode decomposition. Methods of Information in Medicine, 43(1): 60-65. https://doi.org/10.1267/METH04010060

[3] Janosi, I.M., Muller, R. (2005). Empirical mode decomposition and correlation properties of long daily ozone records. Physical Review E, 71, 056126. https://doi.org/10.1103/PhysRevE.71.056126

[4] Kerschen, G., Vakakis, A.F., Lee, Y.S., McFarland, D.M., Bergman, L.A. (2006). Toward a fundamental understanding of the Hilbert-Huang transform in nonlinear structural dynamics. Proceedings of the 24th International Modal Analysis Conference (IMAC), St-Louis.

[5] Khelif, A.M., Cherif, B.D.E., Bendiabdellah, A. (2018). Diagnosis of SVM controlled three-phase rectifier using mean value of park currents technique. International Review on Modelling and Simulations (IREMOS), 11(2): 93-101. https://doi.org/10.15866/iremos.v11i2.13848

[6] Zhang, J.H., Luo, H., Zhao, J., Wu, F. (2015). A fuzzy-based approach for open-transistor fault diagnosis in voltage-source inverter induction motor drives. The European Physical Journal Applied Physics, 69(2). https://doi.org/10.1051/epjap/2015140066

[7] Raj, N., Mathew, J., Jagadanand, G., George, S. (2016). Open-transistor fault detection and diagnosis based on current trajectory in a two-level voltage source inverter. Procedia Technology, 25: 669-675. https://doi.org/10.1016/j.protcy.2016.08.159

[8] Ouanas, A., Medoued, A., Salim, H., Mordjaoui, M., Sayad, D. (2018). Automatic and online detection of rotor fault state. International Journal of Renewable Energy Development, 7(1): 43-52. https://doi.org/10.14710/ijred.7.1.43-52

[9] Rabah, A., Abdelhafid, K., Azeddine, B., Ziane, D. (2018). Rolling bearing fault diagnosis based on an improved denoising method using the complete ensemble empirical mode decomposition and the optimized thresholding operation. IEEE Sensors Journal, 18(17): 7166-7172. https://doi.org/10.1109/JSEN.2018.2853136

[10] Wu, Z.H., Huang, N. (2011). Ensemble empirical mode decomposition: A noise-assisted data analysis method. Advances in Adaptive Data Analysis, 1(1): 385-388. https://doi.org/10.1142/S1793536909000047

[11] Xue, X.M., Zhou, J.Z., Xu, Y.H., Zhu, W.L., Li, C.S. (2015). An adaptively fast ensemble empirical mode decomposition method and its applications to rolling element bearing fault diagnosis. Mechanical Systems and Signal Processing, 62-63: 444-459. https://doi.org/10.1016/j.ymssp.2015.03.002

[12] Cherif, B.D.E., Bendiabdellah, A. (2018). Detection of two-level inverter open-circuit fault using a combined DWT-NN approach. Journal of Control Science and Engineering (JCSE), Volume 2018. https://doi.org/10.1155/2018/1976836